Dynamics of Atmospheres and Oceans, 2 (1977) 1—18

AXISYMMETRIC CRITICAL WITHDRAWAL OF A ROTATING FLUID

JOHN A. WHITEHEAD Jr. and DAVID L. PORTER

Woods Hole Oceanographic Institution, Woods Hole, Mass. 02543 (U.S.A.)

(Received March 11, 1977; accepted May 7, 1977)

ABSTRACT

Whitehead Jr., J.A. and Porter, D.L., 1977. Axisymmetric critical withdrawal of a rotating fluid. Dyn. Atmos. Oceans, 2: 1—18.

The problem of inertial critical flow out of a rotating cylindrical container is addressed theoretically and experimentally. The inviscid steady-state Navier—Stokes equations with the approximation of no vertical shear and the hydrostatic approximation are solved by closing the problem with a critical condition which is applied at the radius of the exit sink. Although the results are presented in general, attention is focused upon the problem when the exit radius is less than the source radius, in which case rotation can be important even when the apparatus size is much less than the Rossby radius of deformation. The results of the analysis are compared to experiments to see if the assumptions were justified. The experiment leads to results that agree closely with predictions of the theory. However, one result is gleaned from the experiment which the theoretical results did not predict. It is that an instability in the flow occurs and is manifested as an azimuthally traveling wave. The role of axisymmetry in producing intense rotational effects is discussed in context with the experimental findings, and possible implications to withdrawal of oceanic waters by ocean thermal difference power plants are discussed.

1. INTRODUCTION

Frequently when one attempts to empty a bottle of water rapidly, one automatically swirls the water in the inverted bottle causing the fluid to be held up to the sides by centrifugal force as it spins around, thereby allowing air to easily enter the bottle. We see the same centrifugal force commonly spin water about the drain of a basin as it empties. In both cases the free surface intersects the drain hole, and hence a free parameter is introduced into the problem so that the problem must be cast as one involving "critical flow."

One of the simplest examples of such a rotating critical flow can be found in the case in which fluid commences to empty out of a hole in the center of a rotating cylindrical container of fluid whose axis is aligned with gravity and the rotation vector. Starting from a state of rest in the rotating frame after the hole is opened, the fluid soon begins to rotate over the exit hole, and

shortly thereafter the free surface of the fluid rapidly pitches downward into the hole, so that the free surface forms a dynamic barrier to the exiting fluid. At this stage the mass flux out of the hole is "critically controlled" by the surface of the fluid (Rouse, 1961).

We have been led to a study of such flows in a rotating frame for two reasons. The first is because of their possible application to geophysical problems. Some of the proposed oceanic thermal difference power plants (Anderson and Anderson Jr., 1966: Zener, 1973) for instance, will withdraw relatively great amounts of water from the depths of the ocean, and it is necessary to determine whether the volumes presently envisaged will result in significant swirling about the entrance hole with an accompanying depression or elevation of the thermocline. The results to be presented here indicate that such swirling will occur, with accompanying depression and/or elevation of up to hundreds of meters. Elsewhere in nature, there are other vortices which may be controlled in part by hydraulic critical principles, such as the eye of a hurricane, the region around a tornado funnel, and the deep convection events which form Mediterranean bottom water during cold winter winds. Such applications will not be studied here, but the theoretical section might provide a foundation for later work along this line.

During the present decade there have been many studies made into the role of radial mass flux in the Ekman layers which border geostrophic interior flows. The present study differs from those in that the radial flux is provided by nonlinear effects in the interior. These effects are expected to be dominant when the Rossby number is sufficiently large compared to the Ekman number. The present studies resemble most closely the study of swirling flows in a pipe by Binnie (1949), although the geometry is somewhat different, and the study of potential outflow by Chisnell (1966), although the effect of a free surface critical flow was not studied there.

The second reason for this study is to make experimental observations of a rotating critical flow in the limit of rapid rotation. Although this subject has recently been attacked theoretically (Stern, 1972; Whitehead et al., 1974; Stern, 1974; Sambuco, 1975; Sambuco and Whitehead, 1976), extensive experiments have not yet been conducted in the rapid rotation limit, due to experimental problems in the various geometries. Hence, questions have arisen about the role of Ekman layers, the stability of the flow, and the appropriateness of using quasi-geostrophic equations for a strongly nonlinear problem. The present geometry has allowed us to conduct experiments in a parameter range where rotation is an important constraint so that the above questions can be addressed more completely than in earlier studies.

In section 2 we will formulate and solve the simple problem of the flow of a uniform density fluid which is introduced at one radius and critically withdrawn at another radius in a cylindrical container. The predictions will be compared with laboratory measurements in section 3, in the course of which good agreement will be reported between experiment and the theory except in one parameter range where an instability to the axisymmetric state will

be described. In section 4, some laboratory observations of nonaxisymmetric withdrawal will be reported. A brief summary and discussion will be made in section 5, followed by some numerical estimates in part 6.

2. A THEORETICAL MODEL

A simple theoretical solution will be presented in this section both in order to have a theoretical prediction for comparison with experiments and to present the dynamical predictions for later applications. Our purpose is to analyze nonlinear axisymmetric flow of an inviscid homogeneous fluid in a rotating frame. In order to simulate conditions which might be geophysically relevant, the fluid, of density ρ_0, will lie under a deep, stagnant fluid of density $\rho_0 - \Delta\rho$.

The geometry will consist of a cylindrical container with a flat bottom in uniform rotation with an axisymmetric source of fluid at radius r_1. The velocity of this fluid will be set at v_1 in an azimuthal direction and u_1 in a radial direction with respect to the frame of rotation. The height of the fluid will be called h_1 at r_1. At another radius, which can be greater or less than r_1, an axisymmetric sink of infinite capacity (such as a hole) will exist.

The pressure in the upper fluid will be:

$$P(z) = -g(\rho_0 - \Delta\rho)(z - H) + (\rho_0 - \Delta\rho)\frac{f^2r^2}{8}$$

where $f = 2\Omega$ is the Coriolis parameter, H is an arbitrary height of the surface of the stagnant fluid at $r = 0$, z is the vertical coordinate, r is the radial coordinate, and g is the force of gravity. The interface between the bottom and top fluid will be given by:

$$z = h(r)$$

and no fluid flows through this interface, hence:

$$u\frac{\partial h}{\partial r} = w(h)$$

where u and w are radial and vertical velocities of the lower fluid. Throughout, we will only consider axisymmetric flows. The equation of continuity and the steady inviscid Navier–Stokes equation for the lower fluid are:

$$\frac{1}{r}\frac{\partial}{\partial r}ru + \frac{\partial w}{\partial z} = 0$$

$$u\frac{\partial u}{\partial r} + w\frac{\partial u}{\partial z} - \frac{v^2}{r} - fv = -\frac{1}{\rho_0}\frac{\partial}{\partial r}\left(p - \rho_0\frac{f^2r^2}{8}\right)$$

$$u\frac{\partial v}{\partial r} + w\frac{\partial v}{\partial z} + \frac{uv}{r} + fu = 0$$

$$u\frac{\partial w}{\partial r} + w\frac{\partial w}{\partial z} = -\frac{1}{\rho_0}\frac{\partial p}{\partial z} - g$$

where v is the azimuthal velocity of the fluid.

We have not been able to solve this set of equations completely, but can solve a set based upon the hydrostatic approximation. To see when this is valid, we will rescale $h = \epsilon h'$, $z = \epsilon z'$, $w = \epsilon w'$. The only equation which is changed by the rescaling, short of having primed w, z, and h, is the vertical momentum equation, which now reads:

$$\epsilon^2 \left(u \frac{\partial w'}{\partial r} + w' \frac{\partial w'}{\partial z'} \right) = -\frac{1}{\rho_0} \frac{\partial p}{\partial z'} - g\epsilon$$

It will now be assumed that ϵ is small and we will neglect the term multiplied by ϵ^2. This is the only term which needs to be neglected, and it can be done when the vertical length scale is much less than the horizontal length scale. Reverting back to the unprimed system with the ϵ^2 term deleted, solutions of the form:

$$u = u(r)$$

$$v = v(r)$$

$$w = w(r)z/h(r)$$

$$p = -\rho_0 gz + g\Delta\rho h(r) + \frac{f^2 r^2 (\rho_0 - \Delta\rho)}{8}$$

satisfy the inviscid Navier—Stokes equations, and when they are substituted into the previous set of equations they become:

$$\frac{\partial}{\partial r}(ruh) = 0 \tag{1}$$

$$-fv + u \frac{\partial u}{\partial r} - \frac{v^2}{r} = -g' \frac{\partial}{\partial r} \left(h - \frac{f^2 r^2}{8g} \right) \tag{2}$$

$$u \left(\frac{\partial v}{\partial r} + \frac{v}{r} + f \right) = 0 \tag{3}$$

where $g' \equiv \Delta\rho$

The continuity and interfacial kinematic condition have been combined to give eq. 1. It has not been necessary to make either a depth-averaging approximation or the Boussinesq approximation to get this far. In fact, our experiments will be conducted in a situation in which $\Delta\rho \simeq \rho_0$.

Since the fluid always flows from the source to the sink, $u \neq 0$, and hence eq. 3 leads to a relation governing v that, when integrated, leads to:

$$v = \frac{c}{r} - \frac{fr}{2} \tag{4}$$

Note that this consists of a potential vortex (with zero vorticity everywhere) plus rigid body rotation. Setting $v = v_1$ at $r = r_1$, we find:

$$c = v_1 r_1 + \frac{f r_1^2}{2} \tag{5}$$

Note that with this solution the neglected viscous term $\nabla^2 v$ would vanish identically. Eqs. 2 and 3 are combined and integrated from r_1 to r to find Bernoulli's law:

$$\frac{u^2+v^2}{2}+g'\left(h-\frac{f^2r^2}{8g}\right)=\frac{u_1^2+v_1^2}{2}+g'\left(h_1-\frac{f^2r_1^2}{8g}\right) \tag{6}$$

Eqs. 4, 5, and 6 can be used to solve for:

$$u^2=2g'(h_1-h)+u_1^2+v_1^2-\frac{\left(v_1r_1+\frac{fr_1^2}{2}\right)^2}{r^2}+v_1r_1f+\frac{f^2r_1^2}{2}-\frac{f^2r^2}{4}$$

$$-\frac{2f^2r_1^2g'}{8g}+\frac{2f^2r^2g'}{8g} \tag{7}$$

Using

$$u=\frac{Q}{2\pi rh}$$

where Q is total (known) mass flux, we find:

$$g'h^3-g'Hh^2+\frac{Q^2}{8\pi^2r^2}=0 \tag{8}$$

where:

$$H=h_1+\frac{u_1^2+v_1^2+v_1r_1f+\frac{f^2r_1^2}{2}}{2g'}-\frac{\left(v_1r_1+\frac{fr_1^2}{2}\right)^2}{2g'r^2}$$

$$-\frac{f^2r^2}{8}\left(\frac{1}{g'}-\frac{1}{g}\right)-\frac{f^2r_1^2}{8g} \tag{9}$$

Eq. 8 is in the same form as the equation for the inertial withdrawal of a nonrotating fluid from a cylindrical container, except that in this case the potential head given by eq. 9 varies with r.

One can see some features of the solution by inspecting the shape of the free surface height h and the Bernoulli potential as a function of r/r_1. To accomplish this, the dependent variables will be represented by the dimensionless Froude number:

$$F\equiv u_1/(2g'h_1)^{1/2}$$

and the Rossby radius of deformation:

$$R\equiv(g'h_1/f^2)^{1/2} \tag{10}$$

The cubic eq. 8 was solved for $h(r)$ with $g' = g$ and plotted in Figs. 1 and 2 as a heavy line. The Bernoulli potential also varies with r, and was plotted as a lighter line. Only in the case $g' = g$ does the potential approach a constant as $r \to \infty$, otherwise it decreases through zero at sufficiently large r. Fig. 1 corresponds to the flow regime when $r_1/R = 10.0$ (corresponding to a relatively strong rotational constraint) and Fig. 2 when $r_1/R = 0.1$ (corresponding to a relatively weak rotational constraint). The letters a, b, c, and d in each graph refer to the different Froude numbers 2, 1, 0.5, and 0.1, respectively. When one traces out the solution by starting at $h/h_1 = 1$ and $r/r_1 = 1$ and decreasing r/r_1, a point of infinite slope is reached as designated

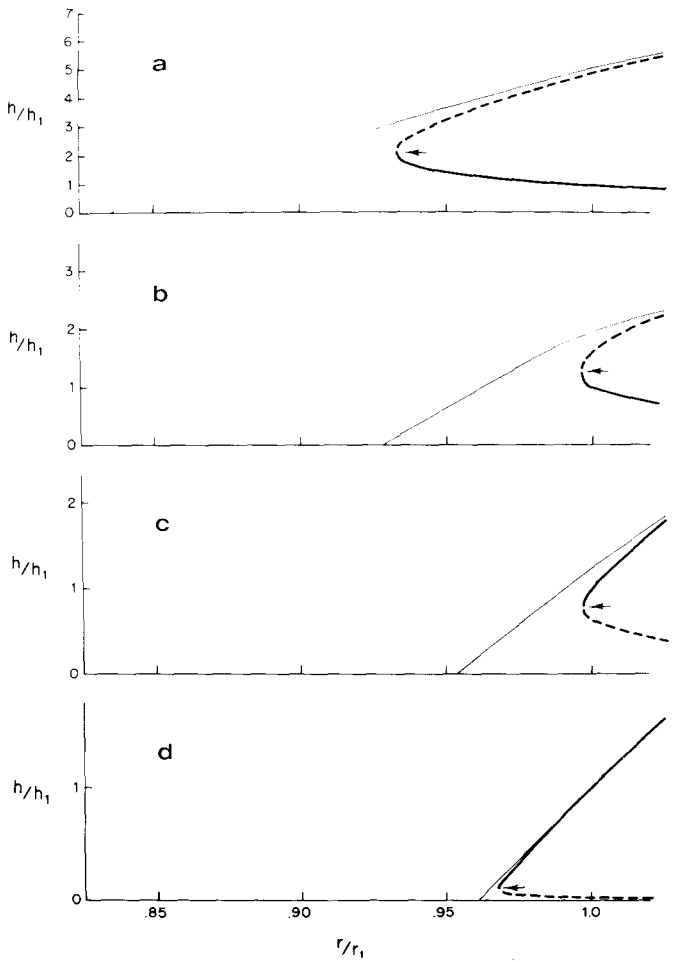

Fig. 1. Trajectories of h/h_1 (heavy solid and dashed lines) as a function of r/r_1 for the case of $r_1/R = 10.0$ and F = 2, 1, 0.5, and 0.1 as a, b, c, and d, respectively. The thin solid line is the Bernoulli head.

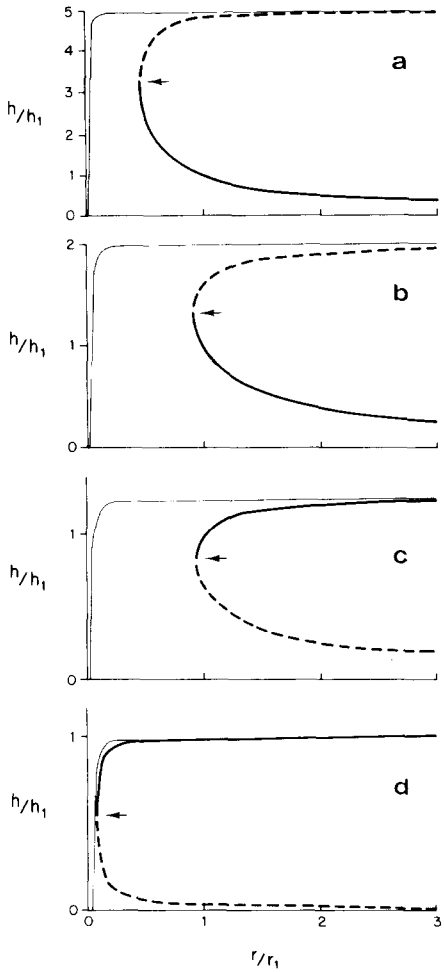

Fig. 2. Trajectories of h/h_1 (heavy solid and dashed lines) as a function of r/r_1 for the case of r_1/R = 0.1 and F = 2, 1, 0.05, and 0.1 as *a*, *b*, *c*, and *d*, respectively. The thin solid line is the Bernoulli head.

by an arrow. Beyond that the height has been drawn with dashed lines, as it is difficult to see how a flow could get to this state.

An unexpected feature is that if all the solutions were plotted on the same graph it would be easily seen that a forbidden region in solution space is bounded by the line $h/h_1 = 1$ in the domain $r/r_1 = [1,\infty]$ and by the curve $h/h_1 = r_1/r$ in the domain $r/r_1 = [1,\infty]$.

Fig. 1 shows that there is only a narrow range of r/r_1 in the domain $r/r_1 = [0,1]$ which has a positive Bernoulli head. In this limit the theory approaches the wide-weir result of Sambuco and Whitehead (1976). In the second extreme case (Fig. 2), $R >> r_1$ so there is no effect of rotation

except in a small region near $r/r_1 = 0$. Assuming $u_1 = v_1 = 0$, one can determine the width of this region by setting $H = 0$ for small r in eq. 9. The width is approximately equal to:

$$r \simeq r_1^2/2\sqrt{2}R \tag{11}$$

This shows that one can always get a "bathtub" vortex for small f given a drain with sufficiently small radius.

Solutions were also obtained for the case in which $g \neq g'$. This causes the Bernoulli head, H, to be a curve which rises through zero to some maximum and then falls back through zero as r is increased. The function $r(h)$ has become multivalued. Further solutions can be easily obtained by numerical solutions of eqs. 8 and 9.

Fortunately it is not necessary to invert the cubic eq. 8 in general to determine the mass flux properties of the system. To determine these properties, it is important to note that trajectories of the solution cannot extend to all values of r, and there is some radius where r reaches its extremum, at which point $\partial r/\partial h = 0$. Taking $\partial/\partial h$ of eq. 8, it is easy to show that when $\partial r/\partial h = 0$ it is necessary that:

$$h = \tfrac{2}{3}H$$

The values of r, h, and H at which this occurs will be called r_0, h_0, and H_0 respectively. We will now invoke a theory of critical control by saying that r_0 is the *radius* of the sink and therefore:

$$h(r_0) = \frac{2H(r_0)}{3} \tag{12}$$

Note that this is the same critical condition which has been derived for non-rotating channel flows. This essentially completes the problem and one of the purposes of the experiments will be to test this control statement.

Eq. 12 allows us to calculate a relation between mass flux and the external parameters v_1, u_1, f, g', r_1, r_0, and h_1, through the use of eqs. 8 and 12 as:

$$Q = 2\pi r_0(\tfrac{2}{3}H_0)^{3/2}\sqrt{g'} \tag{13}$$

where H_0 is found by the use of eq. 9 with $r = r_0$. A simple limit exists when $v_1 = 0$ and u_1 contributes a negligible amount to the Bernoulli potential at r_1. In that case:

$$Q = Q_n \left[1 - \frac{r_1^2}{8R^2}\left\{\gamma^2\left(1 - \frac{g'}{g}\right) + \frac{g'}{g} - 2 + \gamma^{-2}\right\}\right]^{3/2} \tag{14}$$

where:

$$\gamma = r_0/r_1$$

$$Q_n = 2\pi r_0(\tfrac{2}{3}h_1)^{3/2}\sqrt{g'}$$

and we remind you that:

$R = (g'h_1/f^2)^{1/2}$

Q_n is the mass flux for the classical nonrotating critical flow problem. We note that the rotational correction can be large under some circumstances. When this problem is solved in a nonrotating frame, and when v_1 is replaced by $v_1 + fr_1/2$, the answer is not identical to the above. This discrepancy arises solely from pressure due to centrifugal force in the upper stagnant fluid and one of the terms in eq. 14 is missing. This difference can sometimes be very important.

3. EXPERIMENTAL OBSERVATIONS

An experiment was performed to test the validity of the theory in the previous section. As we mentioned earlier, it was felt necessary to do this because a number of assumptions were made such as the shallowness assumption, the critical conditions, and the assumption of no friction. Even if these assumptions are all valid, the previous solution will not exist if it is unstable, and so either theoretical or experimental guidance is needed concerning this possibility.

After inspection of the numerical results which contribute to Figs. 1 and 2, and after examination of the properties of the mass flux prediction in eq. 14, it was decided that the most meaningful, sensitive, and simplest experiment to test the predictions could be conducted in an apparatus with sink radius smaller than the source radius, and with no reduced gravity. The apparatus which was constructed is shown schematically in Fig. 3. It consisted of a cylindrical plexiglass tank with a 39-cm inside diameter, a 15-cm depth, and a 9.6-cm diameter hole labeled R in the center of the bottom. A diffuser labeled Sl with a 30-cm inside diameter was constructed of wire screen, placed in the tank, and stones labeled G of assorted shapes which averaged approximately 1 cm in size were filled into the space between the screen and the outer wall of the tank. Water was fed into the bottom of this rock bed through a loop of 1.8-cm diameter hose labeled O. The loop had approximately 40 holes of 0.5-cm diameter in its side, so that water was fed evenly into the diffuser. The diffuser was effective at producing an axially symmetric velocity at the screen whose vector was normal to the screen.

Below the tank was a catch basin labeled C which contained a submersible pump labeled P whose purpose was to feed water to the upper tank. The entire apparatus was mounted on a turntable, labeled S, which was level to better than 30 sec of arc, so that "tidal" waves in the tank are virtually undetectable with the measuring techniques used.

When the pump and truntable were turned on, water height was measured with a micrometer probe. The probe was mounted on an optical bench which was suspended above the turntable and leveled carefully, so that measurements of the free surface at different radii from the center of the

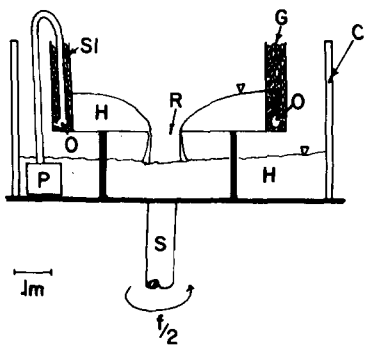

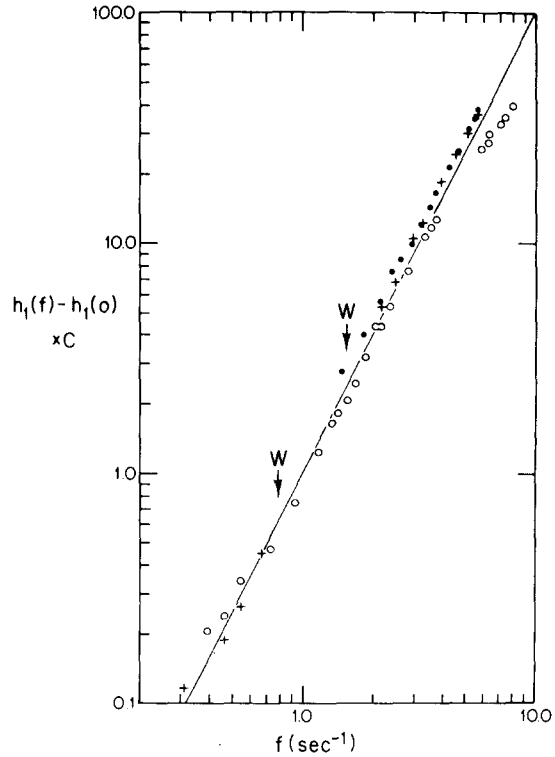

Fig. 3. A cutaway schematic of the apparatus used for the investigation of the theory. The letters reflect the following: H = the fluid; P = the pump; C = the catch basin; SI = the inner screen wall; G = the gravel filler; S = the shaft of the table; O = the loop of feeder hose; and R = the exit hole. The table rotated at frequency $f/2$. Note the shape of the free surface of the fluid in the tank.

Fig. 4. Experimental observations of the height at some rotation rate f minus the height for the same pumping rate at $f = 0$ times a correction factor $C = 8g\, r_0^2/(1 - r_0^2/r_2^2)\,(r_1^4)$. The line is prediction eq. AI-3 which was derived in Appendix I. In all runs the radius of the hole $r_0 = 4.8$ cm, radius of the diffuser $r_1 = 15.0$ cm; (○) —Q = 136 cm^3/sec, r_2 = 13.8 cm where r_2 is radius of the height measuring probe; (●) —Q = 533 cm^3/sec, r_2 = 13.8 cm; (+) —Q = 533 cm^3/sec, $r_2 = 13.3$ cm. The interval between the two W's exhibited a traveling wave on the flow for $Q = 533$ cm^3/sec. The six circles in the upper right may have been influenced by an Ekman-layer flux as discussed in the text.

apparatus could be made and compared to an accuracy better than ±0.005 cm.

The first set of runs were conducted at a constant pumping rate with the rotation rate of the turntable being varied. The probe was located at a fixed radius from the center, and sufficient time was allotted for the height to come to its steady-state value. The data from three runs are shown in Fig. 4. In order for the data to be compared with the prediction in eq. 14, the observed height was subtracted from the height at zero rotation and multi-

plied by the factor $8g\, r_0^2/(1 - r_0^2/r_2^2)(r_1)^4$, where r_1 is the radius of the diffuser and equal to 15 cm, and r_2 is the radius of the probe's position. Derivation of this factor was obtained by solving eq. 14, and will be presented in Appendix I. The line in Fig. 4 corresponds to eq. AI-3 and the predictions are in excellent agreement with the experimental observations.

There were two instances where there was a significant deviation from the predictions, however. In the first instance there are six open circles furthest to the right which have heights substantially below the prediction. In this case, the flux of water outward through the Ekman layer was solved for and it was found that for f above approximately 5 sec^{-1} and Q = 136 cm^2/sec, the Ekman layer has a larger mass flux than the mass flux due to inertial withdrawal. The solution for this Ekman flux is given in Appendix II, and it is interesting to note that height is proportional to f raised to at most a power of 1.5. Since the height due to inertial withdrawal is proportional to f^2, the minimum height for fixed Q as $f \to \infty$ will arise from Ekman flux.

In the second instance between the two places marked with arrows and labeled with the letter W in Fig. 4, a wave travelled around the tank in a prograde direction. This wave was distinct, sizeable in some cases, and most probably is the result of an instability of the axisymmetric fluid flow rather than some mode which is directly forced by the apparatus. To see some of the features of the time-dependent flow observations were made of pressure

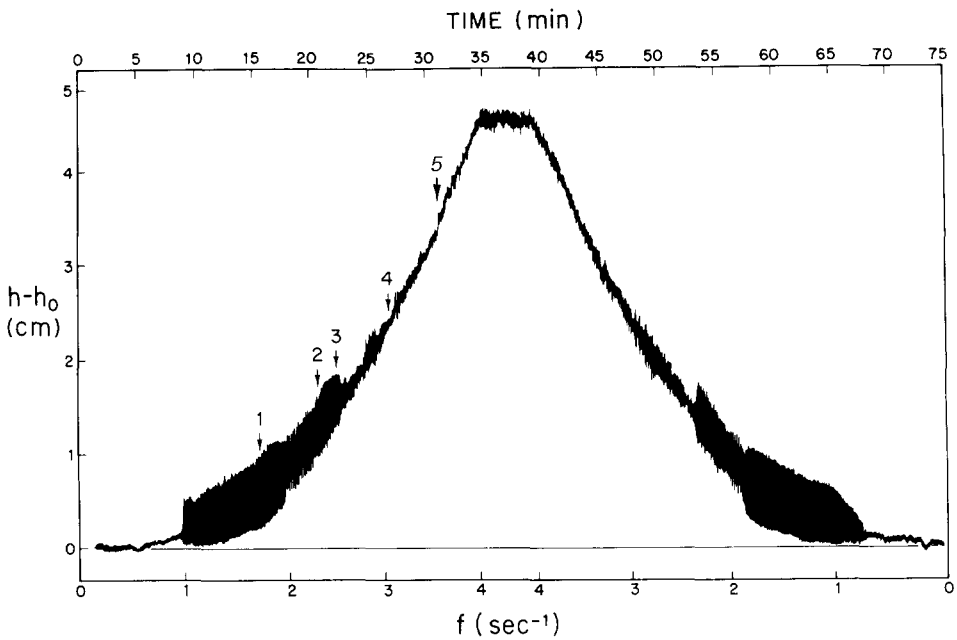

Fig. 5. Height of the free surface as a function of f in an experiment in which f was slowly varied.

at one point with a "tyco" model LP pressure transducer, which is linear to within 1% over its 1-psi pressure range. The transducer was connected to the water with a 2-mm diameter stainless steel tube 23 cm long. A systematic investigation of the time-dependent flow is beyond the scope of this paper, and the data presented here are only intended to give what evidence is presently available that this phenomenon is produced by an instability.

The first evidence is seen by observing the pressure data from an experiment in which f was slowly changed from zero up to 4 sec^{-1} over a span of about 35 minutes, and then slowly changed down again, as shown in Fig. 5. The change in f was performed by manually changing the rotation's speed by small uniform steps every 15 sec. The scale of f is almost but not quite linear, and values of pressure are presented in units of centimeters. For this experiment Q = 533 cm^3/sec. Starting from f = 0, a small increase in head is evident as f is increased. The signal at this frequency is so small that instrumental noise of approximate amplitude 0.5 mm is evident in the record. At approximately f = 1 sec^{-1} there is an abrupt transition to the time-dependent flow that essentially consists of a wave which travels around

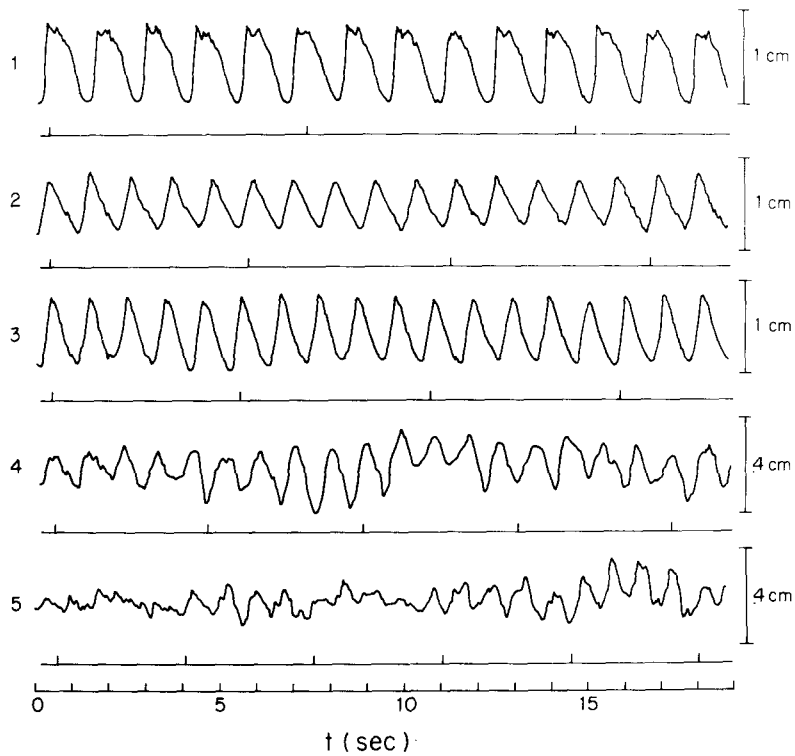

Fig. 6. Curves of pressure versus time at values of f corresponding to the indicated places in Fig. 4. The tick marks below each curve were recorded directly from a switch on the turntable and correspond to one table revolution. The hole was at r_0 = 4.8 cm, the diffuser at r_1 = 15.0 cm and the probe at r_2 = 14 cm.

the tank approximately five times faster than the table. The amplitude of this wave is of the order of the depth of the water. As f is progressively increased, the wave amplitude increases to a maximum at approximately 1.7 sec^{-1}. As f is progressively increased thereafter the amplitude of the time-dependent flow gets smaller and there are a number of apparent "transition points" whose nature has yet to be explored. The curve as f is decreased looks the same with respect to the more prominent "transition points" and the point of maximum amplitude, although the exact value of f where these lie has shifted. This may imply that f has been changed a bit too quickly in our experiment. The time-dependent flow does not go away abruptly at f = 1 sec^{-1}, but continuously decreases its amplitude to a value of zero at about $f = 0.8$ sec^{-1}.

Fig. 6 shows curves of pressure versus time for five values of f that are in the time-dependent region and are labeled consecutively from 1 to 5 on the curve of Fig. 5. These data were taken from different experimental runs that had been allowed to come to steady state before taking recordings. The top curve shows that the wave exhibits characteristics of a finite amplitude shallow water wave, with a steep bore in the front, and a gradually shallowing region behind. There is still no detailed information on the radial dependence of the phase of the wave, but visually it is apparent that the large waves, such as those numbered 1—3 above, have the phase at small radius leading the phase at large radius by as much as 90°. Examination of Fig. 6 will show that there is no phase-locking between the wave and the table, an indication that this is an instability.

4. EXPERIMENTAL EXTENSION

In this section two simple experiments which show some of the distinctive features of the axisymmetric problem will be reported. In the first experiment the height as a function of rotation rate was measured, first in an axisymmetric problem with a small (1.25-cm radius) hole, second in a configuration where one thin plastic wall 1 mm thick extended from the diffuser to the hole. Fig. 7 shows measurements of the height near the diffuser for both cases. The curve A denotes the upstream height as a function of f without the obstructing wall. The difference between the two curves is quite dramatic thereby emphasizing the importance of the symmetry. Various small circular probes were inserted vertically near the exit hole to see how sensitive the flow is to small azimuthal variations, and the upstream height was significantly affected by such probes. As a measure, the probe 2 mm in diameter would decrease the upstream height by 20%, one 6 mm in diameter would decrease the upstream height by 75%.

5. SUMMARY AND DISCUSSION

Rotating critical flow in an axisymmetric cylindrical geometry has some unique aspects. One is that if $r_0 << r_1$ the effects of rotation upon the gross

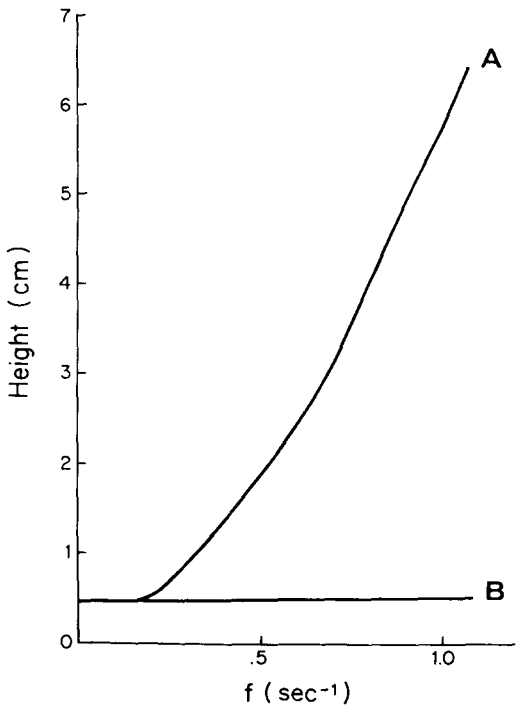

Fig. 7. Curve of height as a function of f in a tank with r_0 = 1.27 cm with radial axisymmetry (A) and a thin wall extending from the diffuser to the hole (B).

mass flux is scaled by the parameters Rr_0/r_1^2, R need not be smaller than r_1 for the rotational effects to be important. This has enabled us to perform simple laboratory experiments which demonstrate significant rotational effects. In one such experiment the upstream height of the fluid was observed to vary markedly with rotation, and to agree well with the prediction eq. AI-3.

The flow which possesses the above features and is perhaps the most familiar to most people is the vortex over a drain. Swirling in this case arises not from a uniform rotation of the container, but rather from the vorticity in upstream eddies. The present study indicates that the intensification of the swirl at the drain does not come from vortex stretching within the drain hole, as many people commonly have suggested, but rather that the intensification comes from the fact that a potential vortex is set up. In fact, vortex stretching is not a viable mechanism in this problem because the fluid within the radius of the drain is moving faster than the critical wave speed, and hence is not able to convey the information of its intensified swirl upstream.

A particularly important limit occurs as the exit hole r_0 goes to zero. A swirling flow develops as r gets less than $r_1^2/2\sqrt{2}\,R$, as stated in eq. 11. The

axisymmetric problem without rotation does not possess this limit and thus is, in a sense, incorrect.

The sensitive dependence upon rotation of this axisymmetric theory carries over to laboratory experiments. Not only was a strong relationship between rotation rate and upstream height observed, but barriers and radially extending walls near the exit radius were observed to decrease this dependence. This may have some utility to engineers who want to prevent the formation of vortices over drains.

This problem is unique from other critical flows in another way — the critical flows can apparently become unstable. The exact nature of the instability has not yet been investigated in detail, but it may be generated by a parametric interaction between the spilling flow and a gravity wave which travels around the tank. Possibly the time-dependent flow receives energy by relaxing the axisymmetric constraint in some way, but at this point we can only speculate. There may be sloshing modes in engineering or geophysics which receive their excitation from the same mechanism.

6. POSSIBLE APPLICATION TO OCEAN THERMAL DIFFERENCE POWER PLANTS

Although the oceanic waters are not comprised of two discrete layers, one moving radially inward to a "sink" while the other lies still, one might hope that the two layer model might possess the same dynamics as a continuously stratified, rotating fluid which is having water withdrawn at a radius r_0. One can approximate the density of a layer of water with the approximation:

$$\Delta\rho = \frac{\partial\rho}{\partial z} h_1 \tag{15}$$

Secondly, one can use the mass flux relation in eq. 14 in the limit $\gamma << 1$, that is:

$$Q = 2\pi r_0 (\tfrac{2}{3}h_1)^{3/2}\sqrt{g'}\left(1 - \frac{r_1^4}{8R^2r_0^2}\right)^{3/2}$$

When the fluid is strongly affected by rotation, that is, when h_1 is much greater than the value it would have if f were zero, everything else being fixed, the relation:

$$r_1^4 = 8R^2r_0^2 \tag{16}$$

almost exactly holds. Given a value of r_0, r_1, and $\partial\rho/\partial z$, one can then determine h_1. Values of r_0 can be obtained from engineering requirements of the ocean thermal difference power plants while $\partial\rho/\partial z$ can be found from oceanographic data. Clearly r_1 cannot be as large as the ocean because this gives values of h_1 which are many times greater than the depth of the ocean. We have solved for r_1 by assumming that at some distance from the source, there is a current of magnitude U which supplies all the water that goes into

the spout of the plant, hence:

$$Q = 2r_1 h_1 U \tag{17}$$

We tested whether our experimental tank would have the same height if fluid came in through only one-fourth the azimuthal area by inserting a baffle around three-quarters of the diffuser. It made little difference to the observed heights. This does not contradict the findings which we reported in section 5 because large changes only occurred when the baffle was placed at a radius smaller than r_1. Values of Q can also be obtained from engineering requirements, while values of U can be obtained from current meter measurements.

Eqs. 15, 16, and 17 can be combined to predict the height h_1, as

$$h_1 = 2^{-7/6} \left(\frac{Q^2 f}{U^2 N r_0} \right)^{1/3}$$

where N is the Brunt-Väisälä frequency, $N \equiv [-(g/\rho_g)(\delta\rho/\delta z)]^{1/2}$. For purposes of these crude computations, we will use $Q = 4500$ m^3/sec, $r_0 = 10$ m, and various values of U and f/N. For a plant located in the Gulf Stream, the values $f/N = 10^{-1}$ and $U = 1$ m/sec lead to a predicted h_1 of 25 m. For a mid-latitude quiet region, the values $f/N = 10^{-1}$ and $U = 0.05$ m/sec leads to $h_1 = 89$ m. Clearly, depressions of isotherms near the bottom intake, or elevations of isotherms near the top intake of these magnitudes could affect the average temperature of the oceanic waters which are driving the power plant, although the existence of these effects in the ocean remains to be tested.

ACKNOWLEDGMENTS

The authors gratefully acknowledge support from the Oceanography Section, National Science Foundation, NSF Grant OCE72-01562 for J.A.W. and from the Ocean Science and Technology Division of the Office of Naval Research, ONR Contract N00014-76-C-0197 NR 083-400 for the support of D.L.P. The experimental apparatus was built with the assistance of Robert Frazel of the Hydrodynamics Laboratory of the Woods Hole Oceanographic Institution. Contribution number 3869 of the Woods Hole Oceanographic Institution.

APPENDIX I: THE CORRECTION FOR MEASURING THE FREE SURFACE AT A RADIUS DIFFERENT FROM THE UPSTREAM RADIUS

To determine this correction it will be pretended that the upstream radius is at the probe and is of radius r_1'. Azimuthal velocity at this radius will be called v_1' and can be determined from eqs. 4 and 5, with azimuthal velocity

at the diffuser zero, to be:

$$v_1' = f\Delta r\left(1 + \frac{\Delta r}{2r_1'}\right) \tag{AI-1}$$

where the radius of the diffuser is r_1 and:

$$\Delta r \equiv r_1 - r_1' \tag{AI-2}$$

With the use of eq. 9, and with the assumption that u_1 is negligible and $g' = g$, one can equate the value of H_0 at some rotation rate f to the value of H_0 at the same mass flux that would exist if $f = 0$, and determine:

$$h_1'(f) - h_1'(0) = \frac{1}{8g}\left(\frac{r_1'^2}{r_0^2} - 1\right)(4v_1'^2 + 4v_1' fr_1 + f^2 r_1^2)$$

where h_1' is the height of the fluid at r_1' or, with the use of eq. AI-1, one can find that:

$$h_1'(f) - h_1'(0) = \frac{f^2}{8g} r_1^4 \left(\frac{1}{r_0^2} - \frac{1}{r_1'^2}\right) \tag{AI-3}$$

The data in Fig. 3 are presented like this, with the correction for the probe placement as determined here.

APPENDIX II: ESTIMATION OF THE MASS FLUX IN THE BOTTOM EKMAN LAYERS

The purpose of this section is to make an estimate of the mass flux in the bottom Ekman layer. It will be assumed that the interior is in geostrophic balance and that the circulation is a potential flow in the interior. Radial mass flux through the Ekman layer is of size:

$$Q = 2\pi r v \delta \tag{AII-1}$$

where:

$$\delta = (\nu/2f)^{1/2}$$

is the effective mass transport depth of the Ekman layer. Since Q must be independent of r:

$$v = \frac{Q}{2\pi\delta r} \tag{AII-2}$$

hence the potential vortex does indeed require no interaction between the Ekman layer and the interior. The height h_1 will now be determined by substituting eq. AII-2 into eq. 2 (in which u is assumed to be zero) and inte-

grating from r_0 (where it will be assumed that $h = 0$) to r_1:

$$-\frac{Qf}{2\pi\delta}\ln(r_1/r_0) + \frac{Q^2}{8\pi^2\delta^2}\left(\frac{1}{r_1^2} - \frac{1}{r_0^2}\right) = -gh_1 + g\frac{f^2(r_1^2 - r_0^2)}{8g} \qquad \text{(AII-3)}$$

which becomes, with the definition of δ:

$$h_1 = \frac{Q}{\sqrt{2}\pi g\sqrt{\nu}}\ln\left(\frac{r_1}{r_0}\right)f^{3/2} + \frac{Q^2 f}{4\pi^2\nu}\left(\frac{1}{r_0^2} - \frac{1}{r_1^2}\right) + \frac{f^2(r_1^2 - r_0^2)}{8g} \qquad \text{(AII-4)}$$

Using a value of $\nu = 0.01$ and the parameters of the experiments, it is straighforward to find that eq. AII-4 will lead to heights which are greater than the inertial heights except for the data where $Q = 136$ cm^3/sec and $f > 6$ sec^{-1}.

REFERENCES

Anderson, J.H. and Anderson Jr., J.H., 1966. Thermal power from sea water. Mech. Eng., 88: 41—46.

Binnie, A.M., 1949. The passage of a perfect fluid throgugh a critical cross-section or "throat". Proc. R. Soc. London, Ser. A., 197: 545—555.

Chisnell, R.H., 1966. Outflow from a circular cylinder under the action of Coriolis force. Tellus, 18: 77—78.

Porter, D., 1977. Instabilities in a Critical Flow Problem. Thesis, M.I.T., Cambridge, Mass., 67 pp.

Rouse, H., 1961. Fluid Mechanics for Hydraulic Engineers. Dover, New York, N.Y., p. 319.

Sambuco, E., 1975. Hydraulic control by a Wide Weir in a Rotating Fluid. Thesis, M.I.T., Cambridge, Mass., 35 pp.

Sambuco, E. and Whitehead, J.A., 1976. Hydraulic control by a wide weir in a rotating fluid. J. Fluid Mech., 73: 521—529.

Stern, M.E., 1972. Hydraulically critical rotating flow. Phys. Fluids, 15 (11): 2062—2064.

Stern, M.E., 1974. Comment on rotating hydraulics. Geophys. Fluid Dyn., 6: 127—130.

Whitehead, J.A., Leetmaa, A. and Knox, R.A., 1974. Rotating hydraulics of strait and sill flows. Geophys. Fluid Dyn., 6: 101—125.

Zener, C., 1973. Solar sea power. Phys. Today, January, pp. 48—53.